

PRODUCTION OF MILLISECOND DIPS IN SCO X-1 COUNT RATES BY DEAD TIME EFFECTS

T. A. JONES¹, A. M. LEVINE², E. H. MORGAN², AND S. RAPPAPORT¹

Submitted to ApJ on September 28, 2007

ABSTRACT

Chang et al. (2006) reported millisecond duration dips in the X-ray intensity of Sco X-1 and attributed them to occultations of the source by small trans-Neptunian objects (TNOs). We have found multiple lines of evidence that these dips are not astronomical in origin, but rather the result of high-energy charged particle events in the *RXTE* PCA detectors. Our analysis of the *RXTE* data indicates that at most 10% of the observed dips in Sco X-1 could be due to occultations by TNOs, and, furthermore, we find no positive or supporting evidence for any of them being due to TNOs. We therefore believe that it is a mistake to conclude that any TNOs have been detected via occultation of Sco X-1.

Subject headings: X-rays: general, X-rays: individual (Sco X-1), solar system: general, Kuiper Belt

1. INTRODUCTION

Chang et al. (2006) found statistically significant 1-2 millisecond duration dips in the count rate during X-ray observations of the bright X-ray source Sco X-1 carried out with the Proportional Counter Array (PCA) on the *Rossi X-ray Timing Explorer* (*RXTE*) and attributed them to occultations of the source by small objects orbiting the Sun beyond the orbit of Neptune, i.e., trans-Neptunian objects (TNOs). In all, Chang et al. (2006) found some 58 dips in approximately 322 ks of Sco X-1 observations. Given that the *RXTE* spacecraft moves through the diffraction-widened shadows of any TNOs at a velocity of $\sim 30 \text{ km s}^{-1}$, dips of $\sim 2 \text{ ms}$ duration should correspond to a TNO size of $\sim 60 \text{ m}$. If the identification of these dips with occultations by TNOs is correct, the dips would provide extremely valuable information on the number and distribution of solar system objects of $\sim 20\text{-}100 \text{ m}$ in size. We have found evidence that these dips are produced by electronic dead-time as a result of high-energy charged particle events in the *RXTE* PCA detectors. Preliminary reports of our results were given by Jones et al. (2006, 2007); herein we give a more detailed and complete report.

2. AVERAGE PROPERTIES OF DIPS IN THE SCO X-1 COUNT RATES

Subsequent to the report by Chang et al. (2006), we searched for dips of the type they describe in the archival data obtained in $\sim 880 \text{ ks}$ of *RXTE*/PCA observations of Sco X-1. These observations were performed starting in early 1996 soon after the launch of the spacecraft. For the search we only used observations that provided count rates of events with a time resolution of $\lesssim 0.25 \text{ ms}$. The total count rate depends on the strength of Sco X-1 at the time of observation as well as on the number of Proportional Counter Units (PCUs) that were operating and the location of the source within the field of view; it ranges from below $40,000 \text{ cts s}^{-1}$ to nearly $200,000 \text{ cts s}^{-1}$ (see Figure 1).

Coincidences within a $\sim 10 \mu\text{s}$ window among two or more of the measurement chains in a Proportional

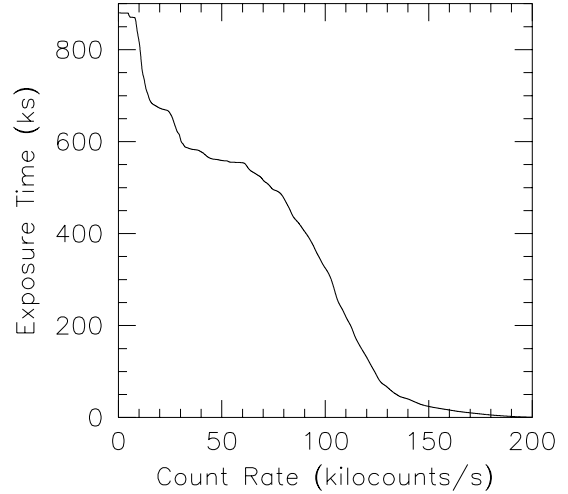


FIG. 1.— Cumulative distribution of exposure time as a function of PCA count rate during observations of Sco X-1 which yielded high time resolution data and were used for the present analysis. The ordinate gives the total exposure time at count rates greater than that of the corresponding rate on the abscissa. Two-LLD events have been included in the count rates when available (see text).

Counter Unit (PCU) are normally used to identify charged particle events (see Jahoda et al. 2006, and references therein, for technical information on the PCA). However, the intensity of Sco X-1 is so high that there is a substantial count rate due to the detection of two X-ray photons in two distinct regions of the detector serviced by different measurement chains within the $10 \mu\text{s}$ window. For most of the Sco X-1 observations, the rates of such so-called two lower-level discriminator (“2-LLD”) events were telemetered with sub-millisecond time resolution. In those cases where the 2-LLD event data are available, we add 2 counts for each 2-LLD event to the counts of single LLD events.

In our search, we looked for instances when the number of counts in a time “window” that is an integral multiple of 0.25 ms (2^{-12} s to be precise) was less than that reasonably expected to occur given the mean count rate. The search was performed for each of the seven window

¹ Department of Physics and Kavli Institute for Astrophysics and Space Research, MIT, Cambridge, MA 02139;

² Kavli Institute for Astrophysics and Space Research, MIT, Cambridge, MA 02139;

intervals of 0.75, 1, 1.5, 2, 2.5, 3, and 4 ms. The expected number of counts in each window was determined from the running average count rate in a time interval centered on the time window of 128 ms for the 0.75 and 1 ms windows, 192 ms for the 1.5 ms window, or 256 ms for the 2, 2.5, 3, and 4 ms windows.

Given N , the number of counts actually measured in the window, and N_{exp} , the expected number of counts in that window based on the running average, we computed $P(n \leq N|N_{exp})$, the probability that N or fewer counts would be detected based on the simplistic assumption that the counts obey a Gaussian distribution with mean N_{exp} and standard deviation $\sqrt{N_{exp}}$. We define the detection of a dip as any instance in which we found $P(n \leq N|N_{exp}) < 10^{-10}$. In the search, the same dip could be found multiple times, e.g., in contiguous intervals when it was longer than the window interval or for different window intervals. We generated a list of 203 dips in which these duplications had been eliminated. Of these, 196 occur in data in which 2-LLD events had been taken into account. All but three of the 58 dips of Chang et al. (2006) and all but 14 of the 107 dips identified by Chang et al. (2007) were identified in our search. Eight of the latter 14 dips were not found by us because we did not search 5 orbits of data that Chang et al. (2007) searched, and because 6 of the 14 did not meet our significance threshold (perhaps because we included 2-LLD events). We detected more dips than Chang et al. (2007) because we included 2-LLD events, because our significance threshold was slightly lower, and possibly because of other minor differences in the searches.

The frequency of occurrence of dips was found to be a function of count rate, and, as one should expect, tended to be higher at the higher count rates. Given our detection criteria, we found no dips at count rates below 43,000 cts s⁻¹ and only three at count rates below 55,000 cts s⁻¹. We searched for dips in data which included approximately 570 ks of observations in which the count rates were above 55,000 cts s⁻¹ (Fig. 1). For each of the seven window durations, we computed N and N_{exp} for window intervals that started every 0.25 ms. Thus the number of independent trials must be less than $7 \times 570,000/0.00025 \sim 1.6 \times 10^{10}$. If the actual probability of finding a dip due to a statistical fluctuation in each trial is $\lesssim 10^{-10}$, then at most a few of the 203 dips could be the result of statistical fluctuations.

In every case, the actual probability of getting N or fewer counts differs from our computed value for at least two reasons. First, the Gaussian distribution we utilized overestimates the probabilities of small numbers of counts by large factors when compared with a Poisson distribution of the same mean. Second, the intensity of Sco X-1 is time variable, and there is some chance that the mean intensity at the time of a dip was lower than that corresponding to N_{exp} . If source variability was important, our detection procedure would have led to numerous spurious detections, particularly for the longer window durations. However, only four dip-like events were most significantly detected when using either the 3 or 4 ms window durations. We further checked the effects of source variability by, first, integrating properly normalized power density spectra of Sco X-1 count rate data over the frequency range of 5-300 Hz, 4-250 Hz,

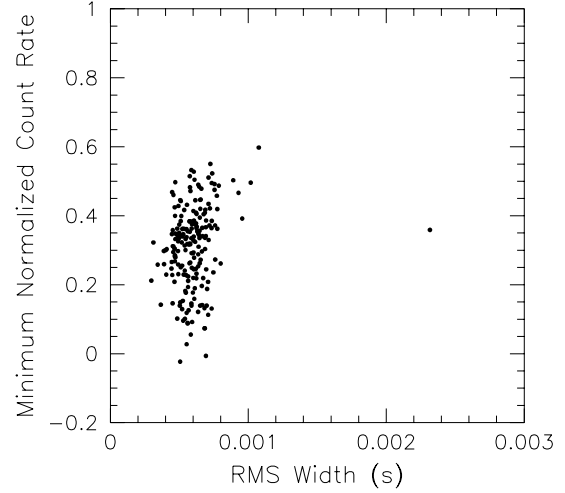


FIG. 2.— Distribution of fitted RMS widths and minimum normalized count rates for 203 detected dip events. The minimum normalized count rate is the value of the model count rate at the center of the fitted Gaussian divided by the average count rate away from the dip.

4-200 Hz, 4-170 Hz, or 4-125 Hz for the 1.5, 2, 2.5, 3, and 4 ms window durations, respectively. The resulting root-mean-square fractional amplitudes in the given frequency bands are typically $\sim 2.5\%$ and are almost always less than $\sim 4.5\%$. These variability estimates for each of the five window durations were then used together with the average count rates on an (*RXTE*) orbit-by-orbit basis to estimate the effects on the dip detection probabilities. The results are consistent with the paucity of dips detected most significantly using the 3 ms and 4 ms window durations and indicate that statistical fluctuations in the presence of source variability did not produce more than ~ 5 spurious detections.

In order to obtain estimates of dip widths and depths, we used the IDL procedure *gaussfit* to fit each dip profile with a function $f(t)$ representing a constant count rate plus a Gaussian shaped dip:

$$f(t) = A - Be^{-(t-t_0)^2/2\sigma^2} \quad (1)$$

where A , B , t_0 , and σ were the parameters to be determined. The values of the fitted widths as parameterized by the values of σ , and of the fitted minimum normalized count rates, i.e., the values of $1 - B/A$, of the ~ 200 dips are shown in Figure 2. The key features of this figure are the relatively narrow range of widths and absence of long dips. Nearly all of the events have $0.4 \leq \sigma \leq 0.8$ ms, and there is only one dip with $\sigma > 1.1$ ms. These aspects of the plot are discussed below (see Section 4).

If the counting rate dips are the result of occultations, then we would expect that diffraction effects would produce small count rate increases on either side of the dips. The sizes of these sidelobes and indeed the other details of the dip profiles depend on a number of factors including the sizes, shapes, distances, and velocities of the occulting bodies, the impact parameters characterizing the occultation events, and the velocities of the *RXTE* spacecraft at the times the dips were observed.

To quantify our expectations of the average diffraction sidelobe size and other typical properties of dips pro-

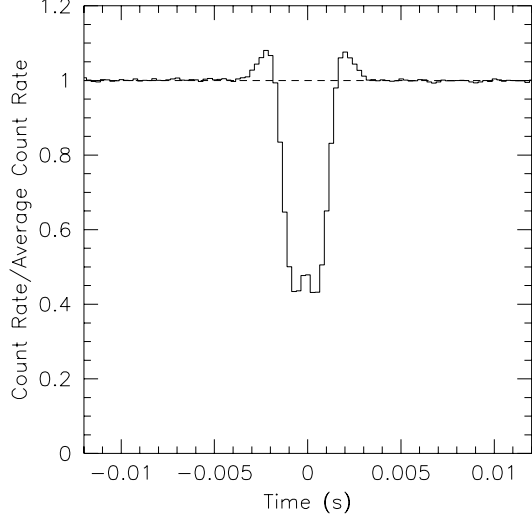


FIG. 3.— Average profile of the 2189 detected 25 km/s model population occultation events. The profiles are superposed after centering and stretching according to the parameters of the fitted Gaussian curves and have been normalized to the count rates at more than 0.007 s from the dip center.

duced by occultations by TNOs, we performed a Monte Carlo computer simulation of an ensemble of occultation events in which the occulting bodies were assumed to be opaque spheres, to have radii s that follow a distribution $\frac{dN}{ds} \sim s^{-4}$, and to follow prograde circular orbits at a distance of 40 AU from the Sun. Since the effects of diffraction are wavelength dependent, we took the spectrum of detected X-rays to be that of a typical pulse height spectrum of Sco X-1 measured with the PCA. The simulation was carried out for each of four cases in which the relative velocity between the spacecraft and the shadows of the occulting bodies was a fixed value, viz. 15, 25, 30, or 35 km s^{-1} .

Simulated dip profiles were computed for a large number of occultations with object size and occultation impact parameter chosen at random according to the appropriate distributions. The profiles were normalized to unity at times far from the occultation centers and were then inserted into the real PCA count rate data by multiplying the actual count rates by the dip profiles. The dip center times were chosen at random among the 880 ks of observations that were used for the present analysis. These data were then searched for dips using the search algorithm described above.

We fit the detected model dips with the function given by eq. (1). The light curves of the PCA data containing the detected simulated dips were superposed after aligning the dip centroids and rescaling the time scale of each light curve in order to normalize all of the fitted widths to the value $\sigma = 0.85$ ms. Interpolation of the rescaled bin times to 0.25 ms time bins was required to superpose the rescaled light curves, and, as a consequence, adjacent bins in the superposition are not completely statistically independent. The results are shown in Figure 3.

The average profile of the real detected dips was similarly constructed by superposing the PCA light curves of 202 of the 203 detected dips after alignment and stretching; the one dip with width $\sigma \sim 2.3$ ms was excluded. The results are shown in Figure 4. To check this, we

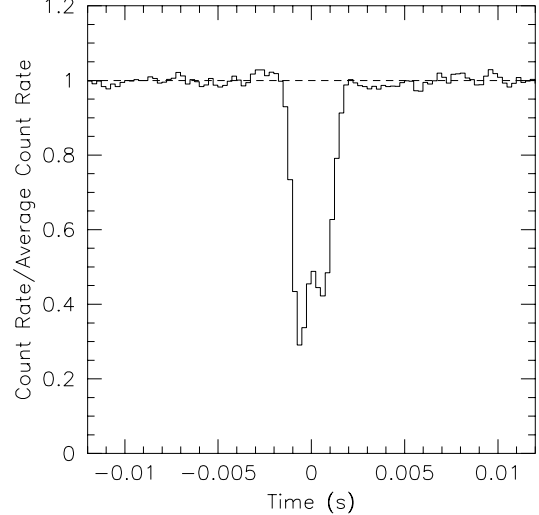


FIG. 4.— Average dip profile of 202 dip events, normalized to the mean count rate at more than 0.007 s from the dip center (dashed line). The standard deviation computed for these bins is 0.016 (1.6% of the count rate).

also superposed only those 109 dips with fitted widths in a narrow range, i.e., with 0.55 ms $< \sigma < 0.75$ ms. The light curves containing those 109 were aligned and summed, but no stretching was done. The results are shown in Figure 5.

Per the results shown in Fig. 3, we expected to see sidelobes with intensities as high as $\sim 8\%$ above the mean count rate determined substantially away from the superposed dips. The superposed light curves do not exhibit diffraction sidelobes as high as those evident in the average profile of the simulated dips, despite having statistics sufficient to reduce fluctuations to $\sim 1.6\%$ (1σ) of the mean count rate. While the differences are not sufficiently significant to be conclusive, they strongly suggest there may be a problem with the occultation hypothesis. We elaborate on this in the discussion section below.

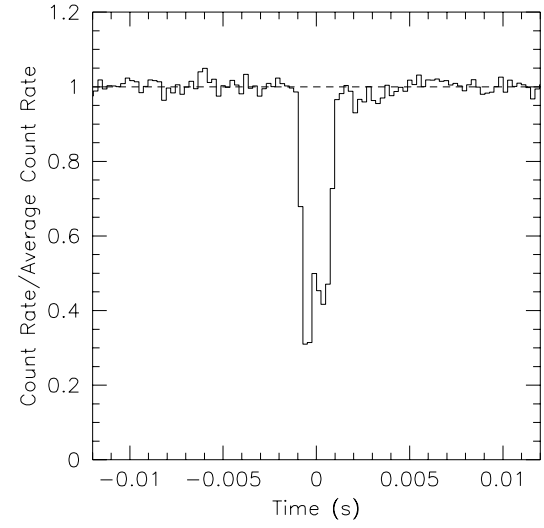


FIG. 5.— Superposition of all 109 events with width parameters between 0.55 and 0.75 ms, with 0.25 ms time bins, normalized to the mean count rate at more than 0.007 s from the dip center (dashed line).

Three additional potential problems with the occultation interpretation are manifest from the dip profiles. First, the summed dip profile is distinctly asymmetric in shape as Chang et al. (2006) suggested for many of the individual dips. Second, the distribution of dip widths is narrower than what one would expect from occultations by bodies with a power-law size distribution of index -4, i.e., there are fewer than expected statistically significant dips with Gaussian FWHM widths greater than ~ 1 ms. Third, when diffraction effects are taken into consideration, one would expect to see a correlation between the fitted widths and the fitted minimum count rates, such that longer dips tend to be deeper on average. No such correlation is seen in Figure 2.

3. SEARCH FOR AN ALTERNATE EXPLANATION

These findings prompted us to further explore alternative explanations for the dips. Only one hypothesis appeared to be worthwhile to pursue, i.e., that the dips are caused by electronic dead time in response to some type of charged particle shower in the spacecraft. Unfortunately, no information with millisecond time resolution was available on the non-X-ray background during the Sco X-1 observations. Counts of good events, very large events (VLEs), propane-layer events, and a catch-all category of other types of events (hereafter SM1-other events) that includes multiple LLD events are available at 1/8 s time resolution from Standard Mode 1; most other types of data are only available with 16-s time resolution.

The VLE flag for a PCU is set when the electronics detect an event in that PCU with energy greater than ~ 100 keV; this can happen in response to the ionization produced by a single charged particle or to that produced by multiple charged particles which penetrate the detector nearly simultaneously. Such a large event can produce ringing in the front-end of an electronic measurement chain. Therefore, in response to the occurrence of a VLE, the digital logic shuts down the electronic processing of events in that PCU for a fixed time period, chosen to be 50 μ s for almost all of these Sco X-1 observations. In addition, each of the 6 main xenon-layer measuring chains is disabled until its charge drops to an acceptable level. In order for the detector to be shut down for an extended period (> 1 ms), an extraordinary amount of charge must be deposited on most of the 6 main measuring chains; it is unclear, at present, whether this can happen in response to a single charged particle.

Figure 6 shows counts of three different types of events from Standard Mode 1 in 1/8-s time bins superposed around the times of 201 dips. In each panel, the centers of the dips have been placed in the bin at $time = 0$. The top panel shows the rates of good events, i.e., those not identified as being due to charged particles, in the main xenon layers of all operating PCUs, and clearly shows the superposed dips; two-LLD events are not included in these rates. The counting rate drops by only $\sim 0.7\%$ because of the dilution of a ~ 2 ms dip within a 128 ms bin. In contrast, the middle panel shows the *enhancement* of the counting rate of SM1-other events in the vicinity of the dips. The peak is highly significant ($\sim 38\sigma$). The bottom panel corresponds to the VLE event rate superposed around the dip times. This peak is also statistically very significant ($\sim 7\sigma$). The increase in the

VLE rate is nearly so large as to be consistent with the detection of ~ 1 VLE per PCU per dip. We discuss this further below.

The enhancements in the SM1-other event and VLE rates around the times of the dips indicate that there is an increase in the rate of detection of non-X-ray events. We speculate that these non-X-ray events interrupt normal event processing for 1-2 milliseconds in most of the PCUs roughly once per hour due to the collection of very large amounts of charge. Such an energetic event may be the consequence of a particle shower produced by the collision of a high-energy cosmic ray with a nucleus in the *RXTE* spacecraft. In any case, further clarification of the causes of the observed dips would be of interest.

4. DISCUSSION

The observed dips have widths and depths that are approximately what one might expect to be produced by occultations by TNOs, even though much wider dips would be detectable in principle (given appropriate depths). Thus we are obligated to seriously consider the hypothesis that some or all of the observed dips are the product of TNO occultations. However, close examination of the *RXTE* PCA data reveals six signatures that independently indicate that few and possibly none of the observed dips are due to occultations by TNOs. The signatures are (1) the numbers of SM1-other events during the dips; (2) the numbers of VLE events during the dips; (3) the absence of the expected diffraction side-lobes; (4) the temporal asymmetry of the dips; (5) the almost total lack of dips longer than ~ 1 ms; and (6) the lack of correlation between dip duration and depth. We discuss each of these in turn.

(1) **SM1-Other Events:** Fig. 6 shows that there is, on average for 201 dips, a large excess of SM1-other events at or near the times of the dips. On average, individual dips should show an excess of SM1-other events at the 2.7σ level. In Fig. 7 we show a histogram of the number of SM1-other events in the 1/8-s time bins corresponding to the dips expressed in standard deviations from the mean. The mean value obtained from the histogram is $\sim 2.7\sigma$, as expected.

If one makes the reasonable assumption that the numbers of SM1-other events should not be affected by true occultations (other than by negligible increases due to reductions in the electronic dead time), then one may estimate the maximum fraction, f_{occ} , of the observed dips that represent genuine occultation events that is consistent with this distribution of SM1-other events. We constructed the following simple function with which to fit the histogram, and thereby constrain f_{occ} :

$$\text{probability} = \frac{1}{\sqrt{2\pi}} f_{occ} e^{-C^2/2} + \frac{1}{\sqrt{2\pi\sigma_{cr}^2}} (1-f_{occ}) e^{-(C-\bar{C}_{cr})^2/2\sigma_{cr}^2} \quad (2)$$

where C is the number of excess SM1-other counts (in units of standard deviations of the counts per bin in each PCA light curve), and \bar{C}_{cr} is the mean of C for those dips which are not the results of occultation events and which we take to be $\approx 2.7/(1-f_{occ})$. The distribution of the numbers of excess SM1-other counts is wider than what would be expected from a Poisson distribution with a mean equal to the slightly increased (on average) number of SM1-other events per bin; the width of this com-

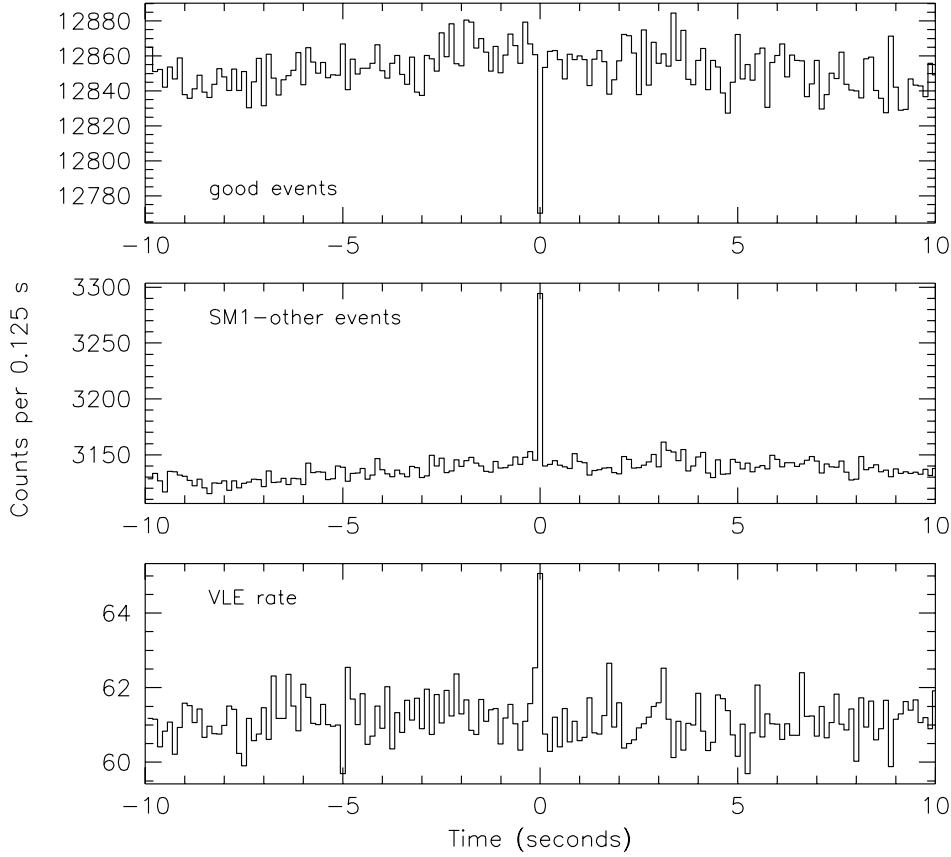


FIG. 6.— Counts per 1/8-s time bin of different types of PCA detector events superposed, i.e., averaged, around the times of 201 dips. The data used for this figure were recorded in Standard Mode 1. The superposition was accomplished such that the bin at *time* = 0 s includes the identified dips. The counts include events from all (typically 3 to 5) of the operating PCUs. Top panel: good xenon counting rate data. The decrease in counting rate due to the dips is apparent. The small ($\sim 0.7\%$) drop in the counting rate is explained in the text. Middle panel: counting rate data of SM1-other events that include multiple-LLD events (see text). A highly significant enhancement in the vicinity of the dips is evident. Bottom panel: VLE event rate data superposed around the dip times, also showing a statistically significant peak. Note that the peak in the VLE event rate is approximately one VLE event per detector per dip event (i.e., ~ 4 excess events per dip).

ponent of the fitting function is adjusted by means of the parameter σ_{cr} . Fits of the function to the histogram in Fig. 7 were carried out with χ^2 fits using both Gaussian and Cash (1979) statistics. If we neglect the tail of the distribution at high numbers of excess SM1-other events, i.e., at $> 9\sigma$, we obtain formally acceptable fits with values of f_{occ} in the range 0.0 to 0.12 and values of σ_{cr} in the range 1.85 to 2.35 (based on Gaussian statistics; the limits represent the formal joint 95% confidence range). Using Cash statistics, we obtain formally acceptable fits with values of f_{occ} in the range 0.0 to 0.11 and values of σ_{cr} in the range 1.65 to 2.15 (95% confidence). These results indicate that fewer than 11% of the 203 dips might be the product of TNO occultations.

(2) **VLE events:** Figure 6 also shows that there is an excess of VLE events around the times of the dips. The difference between the background rate and that in the 1/8-s bin containing the dips is very close to 4 (actually 3.9 ± 0.5) extra VLE events per dip. The peak in Fig. 6 is significant at the 7σ level. If there is precisely one VLE per operating PCU for each non-TNO dip, then we would expect on average an excess of 4.67 VLEs per non-TNO

dip. If only the non-TNO dips contribute to the excess VLE events then there is an upper limit to f_{occ} that is consistent with the observations. If we further allow that the statistical mean excess number of VLE events per dip may have been as small as 2.9, then a simple calculation gives the limit $f_{occ} \lesssim 0.38$ (95% confidence). This limit is weaker than for the SM1-other events, and, furthermore, is compromised by the possibility that more than one VLE event could be produced in a operating PCU in a single cosmic-ray induced dip.

(3) **Lack of diffraction sidelobes:** In Fig. 3 we showed an average profile of simulated dips that had been inserted into actual PCA data. It should be compared to averages of the actual measured dip profiles in Figs. 4 and 5. The average model dip profile shows a clear bump of $\sim 8\%$ amplitude on either side of the dip due to diffraction, whereas the averages of the actual profiles show no significant evidence for diffraction sidelobes. Thus, we conclude that the fraction f_{occ} of legitimate TNO occultations can be no larger than $\sim 30\%$, otherwise diffraction sidelobes likely would have been detected. Again, while this is a clear strike against the dips being due to TNOs,

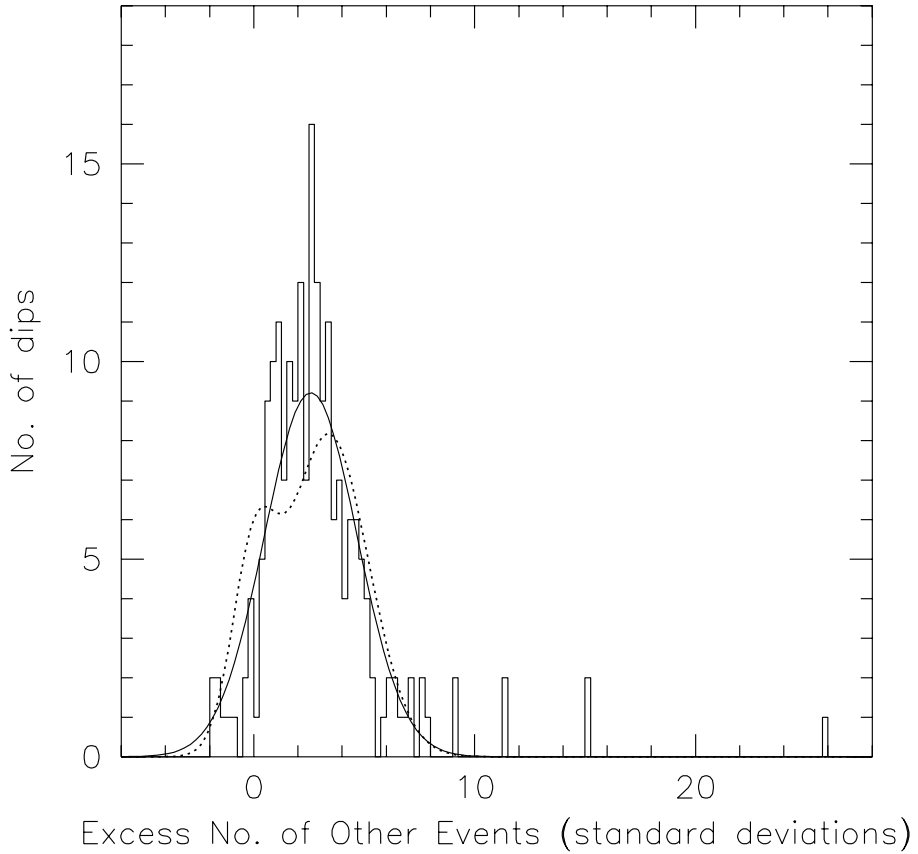


FIG. 7.— Histogram of the numbers of excess SM1-other events in 1/8-s time bins corresponding to the times of 201 of the 203 dips. The number of excess SM1-other events is given in terms of the square root of the mean number of SM1-other events per bin away from the time of the dip. The solid smooth curve represents the best fit with $f_{occ} = 0$, $\sigma_{cr} = 2.1$ and the dashed curve represents a formally unacceptable fit with $f_{occ} = 0.24$, $\sigma_{cr} = 1.8$ (see text).

the limiting statistically significant constraint that can be set due to the lack of diffraction sidelobes is not as significant as for the SM1-other events.

(4) **Asymmetry:** A comparison of the simulated with the actual dip profiles (as in [3]) above, clearly shows a marked asymmetry for the real dip events. This is physically implausible if the dips are the product of occultation events and therefore testifies against a TNO origin for most of the dip events. We estimate that the statistical significance of the asymmetry is $\sim 6\sigma$. Unfortunately, there is no direct way to use this information to constrain the fraction of legitimate TNO occultations. The problem is that we do not know, *a priori*, how large the asymmetry is, on average, for non-TNO dips. Therefore, we can not tell how ‘diluted’ the non-TNO events are by potentially real ones. Nonetheless, this marked asymmetry is another solid indication that few of the dips are the product of TNO occultations.

(5) **Lack of dips longer than ~ 1 ms:** From Fig. 2 we can see that all of the dips, except for a single event, have RMS widths $\sigma < 1.1$ ms. In Section 2 we described a computer simulation of the production, detection, and analysis of dips caused by TNO occultations. For a relative speed between the *RXTE* satellite and the shadows

of the putative TNOs of $v_{rel} = 25$ km s $^{-1}$ we find that the fraction of recovered simulated dips with $\sigma > 1.1$ ms is $\sim 27\%$. For $v_{rel} = 35$ km s $^{-1}$, 9% of the dips have $\sigma > 1.1$ ms. We estimate that the average relative velocity between *RXTE* and the shadows of any TNOs was not higher than $v_{rel} \sim 30$ km s $^{-1}$. For this speed, 16% of the dips are characterized by $\sigma > 1.1$ ms. Therefore, if *all* of the dips are the result of TNO occultations the number of longer-duration dips should be ~ 30 , whereas the observed number is actually 1. On the other hand, if only 15% of the dips are due to TNO occultations, then we would expect only ~ 5 dips with $\sigma > 1.1$ ms. This expected number is marginally statistically consistent, *i.e.*, at $\sim 5\%$ confidence, with the detection of one dip with $\sigma > 1.1$ ms. Therefore, we conclude that the lack of longer dips allows an upper limit of 15% to be set on the fraction, f_{occ} , of potentially real TNO occultations.

(6) **Lack of correlation between width and depth:** If the dips were due to TNO occultations of Sco X-1, we would expect a strong correlation between the widths of the dips and their depths. This results from the fact that diffraction produces shallow occultations for the smaller size occulters, while it produces deeper more geometric-shadowing-like occultations for the larger oc-

culters. As can be seen from the distribution of dip widths vs. depths in Fig. 2, there is no such correlation, with almost all of the dips confined to a narrow range of widths (between 0.4 and 0.8 ms) and depths that range all the way from 45% to nearly 100%. Thus, the fact that the dips we detect include a significant number, i.e., $\sim 20\%$, that are both narrow ($\sigma < 0.7$ ms) and deep (minimum normalized count rate below 0.2) whereas only $\sim 2\%$ of the ‘detected’ simulated dips (for $v_{\text{rel}} \sim 30$ km s $^{-1}$) are this narrow and deep, indicates that $\lesssim 10\%$ of the dips might be due to TNO occultations. Given the effects of statistical fluctuations on the observed number of narrow deep dips and the fact that the simulation is based upon somewhat uncertain parameters, it is more reasonable to use these numbers to set an upper limit of $\sim 20\%$.

Summarizing the results from approaches (1) through (6) above, we find limits on the fraction of valid TNOs to be $f_{\text{occ}} < 11\%$, $< 38\%$, $< 30\%$, $< Q\%$, $< 15\%$, $< 20\%$, respectively, where “Q” denotes that a formal limit could not be set, but the approach provides an important independent indication that the dips are, for the most part, not the result of TNO occultations.

We believe that the combined upper limit on f_{occ} due to the joint application of all six approaches is simply the minimum value achieved by the most sensitive of these, i.e., the constraints cannot be combined. The reason, in short, is that the effects we explore serve only to statistically limit the number of events which could be due to TNOs rather than to identify specific qualifying events. Therefore, our final limit is simply $f_{\text{occ}} \lesssim 10\%$.

One might argue, as did Chang et al. (2007), that since $\sim 10\%$ of the observed dips cannot be formally eliminated as being due to TNOs, they serve as viable potential candidates for TNO detections. However, we argue that if 90% of the dips can be securely eliminated as TNO occultations, and there are six different and independent indicators that point in the direction of a common cause due to cosmic ray interactions in the detector, then it is most plausible that *all* of the dips have this common origin.

While our results cast serious doubt on whether any true occultation events have been detected, one cannot yet conclude with a high degree of confidence that no such events have been detected. Further investigations of the dip phenomenon and its possible causes would be of interest. We are working to obtain a new measurement of, or upper limit on, the rate of occurrence of occultations of Sco X-1 by analyzing the data that are being obtained in a new series of *RXTE* observations of Sco X-1 with high-time-resolution information on VLE events.

5. IMPLICATIONS FOR THE POPULATION OF TNOs

Given that we detected 203 dips in data that covered 570 ks of observations with count rates $\gtrsim 55,000$ cts s $^{-1}$, our upper limit on f_{occ} corresponds to an upper limit of $\lesssim 20$ occultations in the 570 ks of observations. If we adopt a model of the TNO characteristics, this upper limit of detected TNO occultations can be used to establish an upper limit on the abundance of small TNOs. For this purpose we use the assumptions and results of our model TNO simulations described above in Section 2.

A TNO of radius s appears to sweep out a solid angle

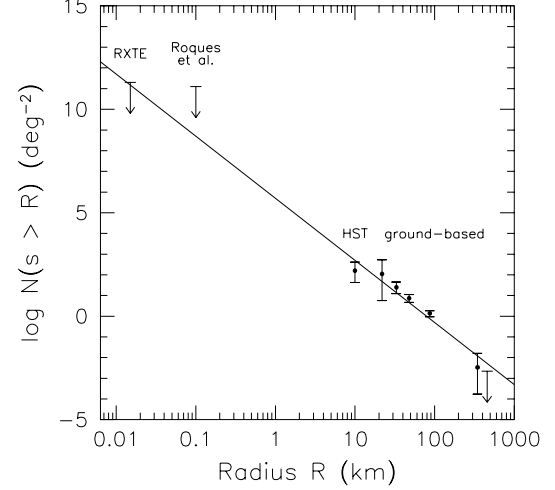


FIG. 8.— Summary of measurements of the cumulative size distribution of small TNOs including the upper limit determined herein from *RXTE* PCA observations. The *HST* and the ground-based optical measurements to the right of the *HST* point have been adapted from Table 2 of Bernstein et al. (2004) by converting limiting R magnitudes to radii by simply scaling from the *HST* limiting magnitude which we take to correspond to a radius of 10 km at a distance of 40 AU. We show error bars that give the ranges of values consistent with Poisson statistics at confidence levels of 90%. The measurements reported in Roques et al. (2006) are shown as an upper limit. The line represents a differential size distribution of $\frac{dN}{ds} \propto s^{-4}$.

per unit time

$$\frac{d\Omega}{dt} = \frac{2(s + \delta)v_{\text{rel}}}{D^2} \quad (3)$$

where $s + \delta$ is the maximum impact parameter for which this body may produce a detectable dip, v_{rel} is the apparent transverse velocity of the TNO, and D is the distance from Earth to the TNO. We find from our simulations of occultations that, on account of diffraction effects, $\delta \sim 7$ m for the model TNOs in the relevant size range. We use $v_{\text{rel}} \sim 30$ km/s and $D \sim 40$ AU. The solid angle swept out in time Δt is

$$\Omega_{sw} = \frac{d\Omega}{dt} \Delta t = \frac{2(s + \delta)v_{\text{rel}}}{D^2} \Delta t. \quad (4)$$

For an ensemble of TNOs of various sizes, the average solid angle swept out per TNO of radius $s > s_{\text{min}}$ is then

$$\overline{\Omega}_{sw} = \frac{1}{N(s > s_{\text{min}})} \int_{s_{\text{min}}}^{\infty} \Omega_{sw}(s) \frac{dN}{ds} ds \quad (5)$$

$$= \frac{2v_{\text{rel}}\Delta t}{D^2} (3s_{\text{min}}/2 + \delta) \quad (6)$$

where we have assumed that the differential size distribution of TNOs is given by $\frac{dN}{ds} \propto s^{-4}$ for $s \gtrsim s_{\text{min}}$. In our simulations we find $s_{\text{min}} \sim 15$ m. Using this and the above values, one obtains

$$\overline{\Omega}_{sw} \sim 2.8 \times 10^{-14} \text{ sr} \sim 9 \times 10^{-11} \text{ deg}^2. \quad (7)$$

Given that as many as 20 TNOs may have been detected, the upper limit on the areal density of TNOs is then

$$N(s \gtrsim 15 \text{ m}) \lesssim \frac{20}{9 \times 10^{-11} \text{ deg}^2} \sim 2 \times 10^{11} \text{ deg}^{-2}. \quad (8)$$

This upper limit may be compared to previous measurements of the size distribution of TNOs at larger radii. Figure 8 summarizes the results of surveys of TNOs smaller than 1000 km. The smallest TNOs which have been securely detected were found in the Hubble Space Telescope ACS survey reported by Bernstein et al. (2004), in which 3 TNOs of radius $s \gtrsim 10$ km were found in 0.019 square degrees of sky. We also show the popula-

tion estimates from ground-based surveys that are summarized in Table 2 of Bernstein et al. (2004).

We are grateful to Jean Swank for helpful discussions on the technical aspects of the PCA and to Jim Elliot for a number of helpful discussions.

REFERENCES

Bernstein, G. M., Trilling, D. E., Allen, R. L., Brown, M. E., Holman, M., & Malhotra, R. 2004, AJ, 128, 1364

Cash, W. 1979, ApJ, 228, 939

Chang, H.-K., King, S.-K., Liang, J.-S., Wu, P.-S., Lin, L. C.-C., & Chiu, J.-L. 2006, Nature, 442, 660

Chang, H.-K., Liang, J.-S., Liu, C.-Y., & King, S.-K. 2007, ArXiv Astrophysics e-prints, arXiv:astro-ph/0701850

Jahoda, K., Markwardt, C. B., Radeva, Y., Rots, A. H., Stark, M. J., Swank, J. H., Strohmayer, T. E., & Zhang, W. 2006, ApJS, 163, 401

Jones, T. A., Levine, A. M., Morgan, E. H., & Rappaport, S. 2006, The Astronomer's Telegram, 949, 1

Jones, T. A., Levine, A. M., Morgan, E. H., & Rappaport, S. 2007, ArXiv Astrophysics e-prints, arXiv:astro-ph/0612129v2

Roques, F., et al. 2006, AJ, 132, 819